Research in Astronomy and Astrophysics, 25:055005 (17pp), 2025 May

https://doi.org/10.1088/1674-4527/adc794
CSTR: 32081.14.RAA.adc794

Optimizing the Input of Liouville Convolution Improves the 10 Day Predictions of Polar Motion

Wei Miao[1,2], Xueqing Xu[1,2], and Yonghong Zhou[1,2]
[1] Shanghai Astronomical Observatory, Chinese Academy of Sciences, Shanghai 200030, China; miaowei@shao.ac.cn
[2] School of Astronomy and Space Science, University of Chinese Academy of Sciences, Beijing 100049, China
Received 2025 January 2; revised 2025 March 22; accepted 2025 March 27; published 2025 May 6

Abstract

This study addresses the critical technical need to enhance the 1–10 day prediction accuracy of polar motion (PM) in satellite autonomous navigation and deep space exploration, with a focus on optimizing the convolution input accuracy within the least squares and autoregression with effective angular momentum (LS+AR+EAM) method. Through theoretical derivation and numerical experiments, we identify the significant impact of the iterative mechanism of the convolution input in the Liouville equation on PM prediction accuracy. On one hand, it clearly states that the initial step of convolution iteration should begin today using today's daily data, rather than relying on the iterative convolution result from the previous step. On the other hand, due to the requirement for the previous PM, previous geodetic angular momentum (GAM), and current GAM in convolution input, several GAM predictions are constructed using IGS ultra-rapid 6 hr resolution data. Additionally, a hybrid method is used to obtain multiple EAM predictions. By integrating these predictions, the range of prediction errors is effectively constrained. The hindcast results, submitted before 20:00 UTC every Wednesday during the official interval of the second Earth Orientation Parameters Prediction Comparison Campaign (2nd EOP PCC), show that the proposed method improved the mean absolute error (MAE) over the first seven days compared to the first-place method (ID136), with improvements of 51.9%, 32.0%, 28.5%, 20.9%, 19.2%, 17.2%, and 17.0% in the *X* direction, and 20.6%, 16.2%, 14.4%, 12.8%, 8.7%, 3.1%, and 3.0% in the *Y* direction. Furthermore, extending the statistical range from 2016/1/6 to 2022/12/28, the proposed method yields MAE values of (0.165, 0.137), (0.735, 0.505), and (1.874, 1.238) mas for days 1, 5, and 10, respectively, outperforming the official predictions by IERS or USNO, which are (0.255, 0.194), (1.534, 1.110), and (2.875, 1.877) mas. This not only validates the stability of the proposed method but also demonstrates its direct applicability in real-world engineering applications.

Key words: astrometry – reference systems – methods: numerical

1. Introduction

Polar motion (PM) is a set of important parameters that describe the Earth's rotational motion, used to depict the changes of the Earth's rotational axis on the Earth's surface, with the *X*-axis pointing toward the prime meridian and the *Y*-axis pointing toward 90° west longitude (Gross 2007). It plays an indispensable role in the transformation between celestial and terrestrial coordinate systems. For instance, applications such as satellite autonomous navigation and positioning, deep space probe operations, astronomical instrument alignment, and satellite orbit determination all require real-time PM. Accurately determining PM parameters requires post-processing of data collected by global space geodetic techniques (Noll 2010; Zajdel et al. 2020, 2021), which results in a delay of several days, making it impossible to obtain real-time PM (Schuh & Behrend 2012). Currently, the EOP C04 series from the International Earth Rotation and Reference Systems Service (IERS) has a delay of 30 days, which is typically filled using the ultra-rapid observed PM resolved by GPS (Mireault et al. 1999; Stamatakos et al. 2009), by using finals.daily updated by United States Naval Observatory (USNO), or by resolving ultra-rapid data through customized combination strategies (Kehm et al. 2023; Kiani Shahvandi et al. 2023). In practical applications, besides filling the delay, it is also necessary to predict future PM. Different users have varying needs for the prediction horizons; if the users frequently update the system, they only need to focus on a 1–10 day prediction. Clearly, the more frequently the system is updated, the higher the accuracy of PM. Therefore, focusing on improving 1–10 day predictions of PM is of significant scientific and practical value in the field of astronomical geodesy.

In PM prediction studies, the least squares extrapolation and autoregressive (LS+AR) combined model (Malkin & Skurikhina 1996; Kosek 2004) due to its simplicity and interpretability is in fact the current default method in the predictions of PM components by the IERS Bulletin-A (Kiani Shahvandi et al. 2022). In fact, the AR model's prediction errors tend to accumulate over time, causing long-term prediction deviations

to grow exponentially. As a result, the LS+AR model is best suited for short-term forecasting horizons. Numerous studies have focused on the LS+AR method, including discussions on input data (Xu & Zhou 2015), periodic amplitude and phase variations (Su et al. 2014; Sun 2020), multi-perspective processing of input data (Miao 2023), integration with singular spectrum analysis (Shen et al. 2018; Jin et al. 2021; Kong et al. 2023a; Wu et al. 2023), integration with Kalman filtering (Xu et al. 2012; Jia et al. 2018), and integration with geophysical excitation functions (Dill et al. 2019; Wu et al. 2022; Kong et al. 2023b; Wei et al. 2024). However, for long-term PM prediction, neural networks have been demonstrated to be the most effective method (Schuh et al. 2002; Wang 2007; Wang et al. 2018; Kiani Shahvandi et al. 2022, 2023, 2024a; Kong et al. 2023b; Wang & Zhang 2023; Wang et al. 2024). By integrating diverse features, neural networks effectively retain memory and maintain accuracy even in long-term prediction horizons.

PM describes the irregular variations of the Earth's instantaneous rotation axis relative to the Earth's surface. These variations include the effects of surface fluid layers, represented by effective angular momentum (EAM), as well as the influence of core dynamics resulting from core-mantle interactions (Kiani Shahvandi et al. 2024a). The first and second Earth Orientation Parameters Prediction Comparison Campaign (1st EOP PCC and 2nd EOP PCC) reached a consensus that using EAM data is crucial for achieving the best 1–10 day prediction accuracy of PM (Kalarus et al. 2010; Kur et al. 2024). The Earth System Modeling Group of GeoForschungsZentrum Potsdam (ESMGFZ) publicly releases the EAM products for the past and the future 6 days (Dobslaw & Dill 2018; Dill et al. 2019, 2021). Based on the EAM data set, Dill et al. (2019) first transferred the geodetic PM domain to the excitation domain through the Liouville equation's deconvolution equation to obtain geodetic angular momentum (GAM). Then, by combining with the EAM in the excitation domain, the geodetic angular momentum residual (GAMr) was obtained. The LS+AR model was used to predict GAMr, and by superimposing the GAMr prediction with the EAM forecast, the predictions for GAM were obtained. Finally, the GAM prediction was transferred to the PM domain through the Liouville equation's convolution equation. This method is referred to as the least squares and autoregression with effective angular momentum (LS+AR+EAM) method and ranked first in the 2nd EOP PCC.

After analyzing the LS+AR+EAM method proposed by Dill et al. (2019), it was found that the deconvolution and convolution of the Liouville equation are critical (Wilson 1985). Among them, the input for convolution requires the previous PM, the previous GAM, and the current GAM. After applying the convolution formula, the first result of the conventional convolution is today's PM, and future PM values are obtained through successive iterative cycles. However, the USNO or IERS updates the rapid PM observations at around 19:00 UTC each day. Therefore, today's PM value should use the updated rapid PM observations, and the result obtained from the conventional convolution should be discarded. Furthermore, in the next step of the convolution during the iterative cycle, today's updated rapid PM observations should be used instead of the result from the previous convolution. This marks the first key finding of this study. Furthermore, the input for the convolution requires the previous PM, the previous GAM, and the current GAM. The previous PM is determined using rapid observations, making the GAM the key factor affecting the convolution precision. Considering that existing research achieved excellent first-day PM prediction accuracy using IGS ultra-rapid data (Wei et al. 2024), we similarly obtained the first-day PM forecast using IGU data and various methods. Simultaneously, various methods were used to acquire the first EAM forecast value in the excitation domain. Then, since GAM is the superposition of EAM and GAMr, predictions for EAM and GAMr are made again based on the first-day prediction of GAM and EAM. Finally, the superimposed and summarized GAM prediction series will provide multiple options for results. At this point, by keeping one value in GAM constant during the convolution process, exponentially increasing convolution results can be obtained. Finally, calculate their mean absolute error (MAE), using the sum of MAE as the objective function to combine and select the best convolution results. Meanwhile, this implies that a relatively better initial value scheme for GAM convolution was found in reverse. Compared to conventional convolution, the new convolution operation method not only takes a step ahead but also optimizes the selection of initial convolution values. This is the second finding of this study.

During the implementation of the experiment, the prediction results were strictly output by Wednesday 20:00 UTC as stipulated by the 2nd EOP PCC. Two prediction accuracy statistical intervals were set: the 2nd EOP PCC (2021 September 1–2022 December 28) and the extended 2nd EOP PCC (2016 January 6–2022 December 28). Not only were GFZ's EAM forecast products evaluated, but ETH's EAM forecast products were also assessed. The results were fairly and impartially compared individually not only with the first place of the 2nd EOP PCC (ID136) but also with the official products of USNO or IERS (ID200).

The structure of this paper is as follows: Section 2 introduces all the data sets used in this study. Section 3 provides a detailed analysis of the convolution process of the Liouville equation and presents the details of the method used in this paper. Section 4 first presents the comparative analysis results for the 2nd EOP PCC interval, followed by results for the extended 2nd EOP PCC interval, and some discussion. Section 5 concludes the study.

2. Data

In this section, the study provides a detailed description of the PM final data, rapid data, geophysical excitation data, and 2nd EOP PCC data sets, offering key details for each data source.

2.1. Polar Motion Final Data

The IERS updates and releases the EOP C04 product, which is the most accurate and stable, twice a week. This product is updated with the International Terrestrial Reference Frame updates, with the latest version being the EOP 20C04 series (Altamimi et al. 2023), and the previous version being the EOP 14C04 series (Bizouard et al. 2019). This product has a 30 day time delay and is typically used as a reference true value for evaluating prediction accuracy. Since this study compares with the 2nd EOP PCC, the EOP 14C04 series is chosen as the reference true value.

2.2. Polar Motion Rapid Data

The USNO releases the PM rapid data product daily (Stamatakos et al. 2009). In this product, data from the past month are used to fill the 30 day delay in the EOP 14C04 final series, and future prediction data are considered the official forecast product of the USNO or IERS, represented as ID200 during the 2nd EOP PCC.

2.3. IGS Ultra-rapid Data

At 15:00 UTC, 21:00 UTC, 03:00 UTC (next day), and 09:00 UTC (next day) daily, the IGS updates its ultra-rapid data (IGU) named sequentially as 12, 18, 00, and 06, with high accuracy (Ray et al. 2017). To strictly adhere to the 20:00 UTC deadline of the 2nd EOP PCC, this study uses IGU values updated before 15:30 UTC for each experiment.

2.4. EAM Data

Currently, the Helmholtz-Centre Potsdam—German Research Centre for Geosciences (GFZ) and Eidgenössische Technische Hochschule Zürich (ETH Zürich) publicly provide free EAM data. Among them, GFZ computes and releases daily the final EAM data, including AAM, OAM, HAM, and SLAM, along with forecast data for the next 6 days (Dobslaw & Dill 2018; Dill et al. 2019, 2021). Based on the GFZ's EAM data, ETH Zürich has not only improved the quality of EAM forecasts using neural networks since 2021 May 20, but also extended the forecast horizons from 6 to 14 days (Kiani Shahvandi et al. 2022, 2023, 2024d).

2.5. 2nd EOP PCC Data

Centrum Badań Kosmicznych Polskiej Akademii Nauk (CBK PAN) is the organizer of the 2nd EOP PCC, with the official competition running from 2021 September 1 to 2022 December 28. The organizers rigorously evaluated the forecasting methods of all participating teams (Śliwińska-Bronowicz et al. 2022), and all competition results were published in the form of the 2nd EOP PCC data set (Śliwińska-Bronowicz et al. 2023).

3. Data Processing and Methods

First, the Liouville equation and its discretized form are described, followed by the first and second analyses of the Liouville equation. In the second analysis, concerning the quality of the convolution's initial value, various combination methods are first employed to predict tomorrow's PM, and based on these results, the convolution's initial value is combined and filtered. Finally, the optimal combination scheme for the X and Y directions in the PM domain is presented, and the forecasting process transitions back to the excitation domain.

3.1. Liouville Equation

The Liouville equation serves as a bridge connecting the geodetic PM observation domain and the geophysical excitation domain (Wilson 1985). The process from the PM domain to the excitation domain is called deconvolution, which is a differential relationship. However, the process from the excitation domain to the PM domain is called convolution, which is an integral relationship. The Liouville geophysical equation can be expressed as

$$\chi(t) = \frac{i}{\sigma_c} \cdot \frac{dp(t)}{dt} + p(t), \tag{1}$$

where $i = \sqrt{-1}$, $p(t) = p_x(t) - i \cdot p_y(t)$, and $p_x(t)$ and $p_y(t)$ are defined positive toward the central Greenwich meridian and 90°W longitude, respectively. For the excitation domain, $\chi(t) = \chi_1(t) + i \cdot \chi_2(t)$. The PM variables $(p_x(t), \ -p_y(t))$ and EAM variables $(\chi_1(t), \ \chi_2(t))$ are measured in a right-handed coordinate system, which is Earth-fixed. The σ_c is the Chandler oscillation frequency and $\sigma_c = 2\pi(1 + i/2Q)/T_c$, where Q and T_c are the quality factor and the Chandler wobble period, valued at 179 and 433, respectively.

In practical operations, $p(t)$ and $\chi(t)$ are equally spaced time series, thus Equation (1) needs to be discretized. Wilson (1985) derived the classical discretized Liouville equation using Fourier transform, transfer functions, and Nyquist plots. The derived deconvolution and convolution formulas are expressed as follows:

$$\chi(t - \frac{\Delta t}{2}) = \frac{i}{\sigma_c \cdot \Delta t} \exp(-\frac{i \cdot \pi \cdot \Delta t}{T_c}) \cdot [p(t) - \exp(i \cdot \sigma_c \cdot \Delta t) \cdot p(t - \Delta t)], \tag{2}$$

$$p(t) = -\frac{i \cdot \sigma_c \cdot \Delta t}{2} \exp(\frac{i \cdot \pi \cdot \Delta t}{T_c}) \cdot [\chi(t) + \chi(t - \Delta t)] + \exp(i \cdot \sigma_c \cdot \Delta t) \cdot p(t - \Delta t), \quad (3)$$

where the main variables have been explained in Equation (1). In this study, since the PM resolution used is 24 hr, the Δt is set to 1.

3.2. First Analysis of Liouville's Equation

For the deconvolution process of Equation (2), $\chi(t - \frac{\Delta t}{2})$ can be obtained through $p(t - \Delta t)$ and $p(t)$. Among them, $p(t - \Delta t)$ and $p(t)$ are observations in the PM domain with high accuracy, so the deconvolution process is not the focus of this study. For the convolution process of Equation (3), $p(t - \Delta t)$ belongs to the PM domain, while $\chi(t)$ and $\chi(t - \Delta t)$ belong to the excitation domain. The choice of $\chi(t)$, $\chi(t - \Delta t)$, and $p(t - \Delta t)$ in the convolution process directly affects the result of the convolution $p(t)$.

The previous deconvolution process can obtain $\chi(t - \frac{\Delta t}{2})$ and its historical values. If a 6 day prediction is made in the excitation domain, prediction values $\overset{\infty}{\chi}(t + \frac{\Delta t}{2})$ $\overset{\infty}{\chi}(t + \frac{3 \cdot \Delta t}{2})$, …, and $\overset{\infty}{\chi}(t + \frac{11 \cdot \Delta t}{2})$ will be added after $\chi(t - \frac{\Delta t}{2})$. It is clear that the value represented in the excitation domain at this time is the MJD at noon, which needs to be interpolated to the MJD at midnight. The corresponding adjustment formula can be written as:

$$\chi(t) = 0.5 \times (\chi(t - \frac{\Delta t}{2}) + \overset{\infty}{\chi}(t + \frac{\Delta t}{2})), \quad (4)$$

$$\overset{\infty}{\chi}(t + \Delta t) = 0.5 \times (\overset{\infty}{\chi}(t + \frac{\Delta t}{2}) + \overset{\infty}{\chi}(t + \frac{3 \cdot \Delta t}{2})), \quad (5)$$

$$\cdots\cdots \quad (6)$$

$$\overset{\infty}{\chi}(t + 5 \cdot \Delta t) = 0.5 \times (\overset{\infty}{\chi}(t + \frac{9 \cdot \Delta t}{2}) + \overset{\infty}{\chi}(t + \frac{11 \cdot \Delta t}{2})), \quad (7)$$

where t represents today, $\overset{\infty}{\chi}$ denotes the prediction value, and χ represents the value in the excitation domain obtained from the observations in the PM domain through deconvolution.

Equation (3) tells us that for the first step of convolution, $p(t)$ can be obtained through $\chi(t)$, $\chi(t - \Delta t)$, and $p(t - \Delta t)$. However, since t is today, the first value $p(t)$ obtained from the convolution is the PM value for today. However, the USNO or IERS updates today's PM value at 19:30 UTC. Clearly, we should discard the first value $p(t)$ obtained from the convolution and instead use the daily PM value updated by the USNO.

For the second step of convolution, the first prediction value $\overset{\infty}{p}(t + \Delta t)$ can be obtained through $\overset{\infty}{\chi}(t + \Delta t)$, $\chi(t)$, and $p(t)$. Here, $\overset{\infty}{\chi}$ and $\overset{\infty}{p}$ represent prediction values. $p(t)$ should replace the daily PM value updated by the USNO, rather than iteratively using the result from the first step of convolution. By analogy, iterate to obtain the target prediction value $\overset{\infty}{p}(t + 2 \cdot \Delta t)$, $\overset{\infty}{p}(t + 3 \cdot \Delta t)$, $\overset{\infty}{p}(t + 4 \cdot \Delta t)$, and $\overset{\infty}{p}(t + 5 \cdot \Delta t)$ in the PM domain. This is the first significant finding of this study. In the full text, the approach based on LS+AR+EAM and using the traditional convolution formula is denoted as A1. It is worth noting that, without considering the details of determining the order of the AR model, the A1 method is a replication of the method proposed by Dill et al. (2019). Similarly, the method based on LS+AR+EAM and using the corrected convolution by this discovery is denoted as A2.

3.3. Second Analysis of Liouville Equation

3.3.1. Analysis of Convolution Process

We continue to focus on the convolution process of Equation (3), which can be expressed as follows when expanded backward.

$$\overset{\infty}{p}(t + \Delta t) = -\frac{i \cdot \sigma_c \cdot \Delta t}{2} \exp(\frac{i \cdot \pi \cdot \Delta t}{T_c}) \cdot [\overset{\infty}{\chi}(t + \Delta t) + \chi(t)] + \exp(i \cdot \sigma_c \cdot \Delta t) \cdot p(t), \quad (8)$$

$$\overset{\infty}{p}(t + 2 \cdot \Delta t) = -\frac{i \cdot \sigma_c \cdot \Delta t}{2} \exp(\frac{i \cdot \pi \cdot \Delta t}{T_c}) \cdot [\overset{\infty}{\chi}(t + 2 \cdot \Delta t) + \overset{\infty}{\chi}(t + \Delta t)] + \exp(i \cdot \sigma_c \cdot \Delta t) \cdot \overset{\infty}{p}(t + \Delta t), \quad (9)$$

$$\cdots\cdots \quad (10)$$

$$\overset{\infty}{p}(t + 5 \cdot \Delta t) = -\frac{i \cdot \sigma_c \cdot \Delta t}{2} \exp(\frac{i \cdot \pi \cdot \Delta t}{T_c}) \cdot [\overset{\infty}{\chi}(t + 5 \cdot \Delta t) + \overset{\infty}{\chi}(t + 4 \cdot \Delta t)] + \exp(i \cdot \sigma_c \cdot \Delta t) \cdot \overset{\infty}{p}(t + 4 \cdot \Delta t), \quad (11)$$

where $\overset{\infty}{p}$ and $\overset{\infty}{\chi}$ represent prediction values, t denotes today, and Δt is assigned a value of 1.

From Equation (8), $\overset{\infty}{\chi}(t + \Delta t)$, $\chi(t)$, and $p(t)$ can yield the first desired prediction value $\overset{\infty}{p}(t + \Delta t)$, where $p(t)$ is a known value. Equations (4) and (5) indicate that $\overset{\infty}{\chi}(t + \Delta t)$ and $\chi(t)$ are related to the prediction value $\overset{\infty}{\chi}(t + \frac{\Delta t}{2})$ in the excitation domain. Therefore, this study proposes isolating the first prediction value $\overset{\infty}{\chi}(t + \frac{\Delta t}{2})$ of the excitation domain for individual analysis.

In the excitation domain, there exists GAM obtained through deconvolution, as well as EAM. The former is derived from geodetic observations, while the latter comes from geophysical model solutions. The relationship between them is as follows

$$\mathrm{GAM} - \mathrm{EAM} \equiv \mathrm{GAMr}, \quad (12)$$

where the lengths of GAM and EAM are always consistent. Both GAM and EAM include $\chi(t)$, $\overset{\infty}{\chi}(t + \Delta t)$, …, $\overset{\infty}{\chi}(t + 5 \cdot \Delta t)$. At this time, the initial convolution values in the excitation domain are $\overset{\infty}{\chi}(t + \Delta t)$ and $\chi(t)$, while in the PM domain, the initial convolution value is $p(t)$.

Table 1
Nine Prediction Schemes for the First-Day Prediction in the Polar Motion Domain

Schemes	Input Data	*X*-direction or *Y*-direction
Scheme 1	IGU	LS+AR method
Scheme 2	IGU	differential LS+AR method before LS
Scheme 3	IGU	differential LS+AR method before AR
Scheme 4	IGU	*Y* or *X* prediction of conventional LS+AR method combined with *Y*–*X* prediction of conventional LS+AR method
Scheme 5	IGU	*Y* or *X* prediction of differential LS+AR method combined with *Y*–*X* prediction of differential LS+AR method
Scheme 6	IGU	*Y* or *X* prediction of conventional LS+AR method combined with *Y*–*X* prediction of differential LS+AR method
Scheme 7	IGU	*Y* or *X* prediction of difference LS+AR method combined with *Y*–*X* prediction of conventional LS+AR method
Scheme 8	/	USNO's 1st forecast
Scheme 9	/	IGS's 1st forecast

However, Figure 1 in Dill et al. (2021) clearly illustrates that there is a systematic error in the atmospheric angular momentum of the excitation domain during the initial days, particularly in the first prediction. Therefore, for the first-day prediction of EAM, the first prediction values of *m*th EAMs are obtained using multiple forecasting methods. Wei et al. (2024) achieved excellent accuracy for the first prediction in the PM domain using IGS ultra-rapid data. Consequently, based on IGS ultra-rapid data, the first prediction values of *n*th GAMs are obtained using multiple forecasting methods. Then, future positions are predicted based on the first prediction. After applying Equation (12), the time series $\chi(t)$, $\overset{\infty}{\chi}(t+\Delta t)$, …, $\overset{\infty}{\chi}(t+5\cdot\Delta t)$ will have m^*n results.

Compared to traditional methods, the proposed method begins its convolution from Equation (8). At this time, the initial values for the convolution of the excitation domain are $\chi(t)$, and $\overset{\infty}{\chi}(t+\Delta t)$ are related to $\overset{\in}{\chi}(t+\frac{\Delta t}{2})$. However, compared to $\overset{\infty}{\chi}(t+\frac{\Delta t}{2})$, since $\overset{\in}{\chi}(t+\frac{\Delta t}{2})$ is predicted separately, it has a large number of results and relatively higher prediction accuracy. This also means that the initial values of the excitation convolution, $\chi(t)$ and $\overset{\infty}{\chi}(t+\Delta t)$, also have a large number of high-precision results.

In summary, compared to traditional methods that start convolution from Equation (3), the newly proposed method begins convolution from Equation (8), advancing by one step. In traditional convolution, all $\overset{\in}{\chi}(t+\frac{\Delta t}{2})$ comes from the first prediction of the excitation domain, while in the newly proposed method, $\overset{\in}{\chi}(t+\frac{\Delta t}{2})$ is a combination from the first predictions of the PM domain and the excitation domain. Below is a detailed description of various prediction methods for $\overset{\in}{\chi}(t+\frac{\Delta t}{2})$ in GAM and EAM.

3.3.2. First Polar Motion Prediction in the Polar Motion Domain

The first prediction for the PM domain is for tomorrow. This study employs LS+AR methods, differencing methods, and their combinations based on the *X*, *Y*, and *Y*–*X* series of PM (Miao 2023). The first two methods can yield three results, while the combination method produces four results.

Table 2
Eight Prediction Schemes for the 1st Prediction of EAM

Schemes	Input Data	*X*-direction or *Y*-direction
Scheme 1	24 hr resolution(1461)	LS+AR method
Scheme 2	24 hr resolution(1461)	differential LS+AR method before LS
Scheme 3	24 hr resolution(1461)	differential LS+AR method before AR
Scheme 4	6 hr resolution(1461)	LS+AR method
Scheme 5	6 hr resolution(1461)	differential LS+AR method before LS
Scheme 6	6 hr resolution(1461)	differential LS+AR method before AR
Scheme 7	/	GFZ's 1st forecast
Scheme 8	/	ETH's 1st forecast

Additionally, consideration is given to the first-day prediction from USNO's finals.daily and the first predicted value provided by IGS when updating the first value at UTC 15:10. Thus, a total of nine results are generated for the first-day prediction in the PM domain. According to Equation (2), there are nine results for the first-day prediction in the PM domain, and therefore, nine results for GAM in the excitation domain. See Table 1.

3.3.3. First EAM Prediction in the Excitation Domain

On one hand, we proceed based on Equation (12) and to maintain consistency with GAM's MJD. On the other hand, we consider the systematic error in the first prediction of EAM updated by GFZ (Dill et al. 2021). Thus, various methods were used for re-modeling to make a first-day prediction for EAM. This includes first-day prediction results based on low-resolution and high-resolution LS+AR methods and differencing methods, as well as the first-day predictions from GFZ and ETH for EAM. Thus, there are a total of eight first-day predictions for the excitation domain EAM. See Table 2.

3.3.4. Prediction Process after Summary

The previous Sections 3.3.1, 3.3.2, and 3.3.3 detailed the second analysis of the Liouville equation in this study, and the following Figure 1 integrates this process. See Figure 1.

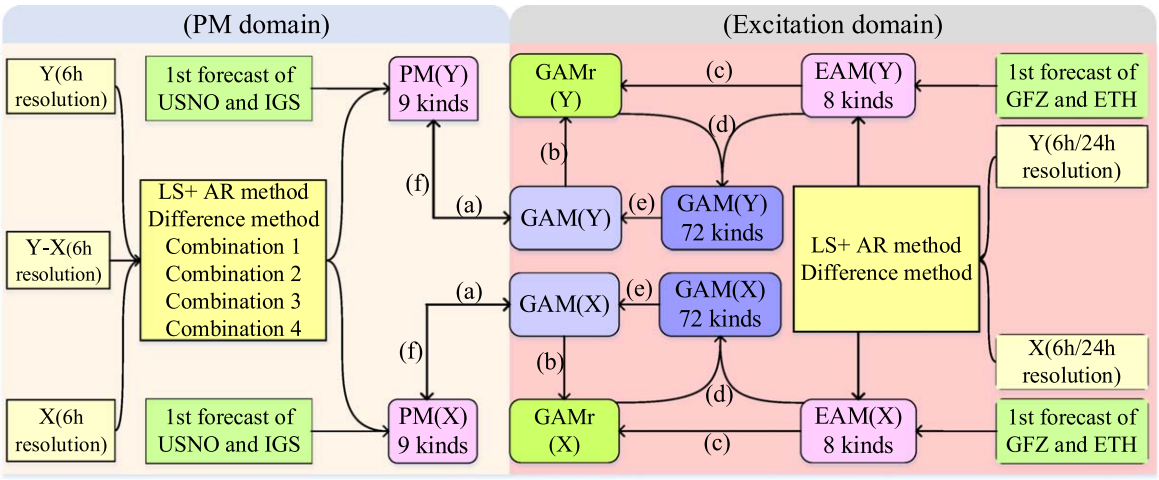

Figure 1. Flowchart of combined methods for prediction in the PM and excitation domains. The left panel corresponds to the schemes in Table 1, and the right panel corresponds to the schemes in Table 2. (a) is the convolution of the predicted 1st day PM values into the excitation domain after splicing; (b) and (c) are the subtraction of GAM and EAM data together to obtain GAMr; (d) is the GAM obtained by adding EAM's 6 day forecast product to GAMr; (e) is the format for adjusting the resolution; (f) is the convolution of the predicted GAM back to the PM domain.

From Figure 1, it can be seen that there are nine types of GAM results and eight types of EAM results obtained. After combining with Equation (12), there are 72 types of GAM prediction results obtained. This means that all prediction values on the right side from Equations (4) to (7) have 72 types of $\overset{\infty}{\chi}$. Meanwhile, all prediction values on the left side from Equations (4) to (7) have 72 types. That is, there are 72 results for $\chi(t)$, $\overset{\infty}{\chi}(t+\Delta t)$, …, $\overset{\infty}{\chi}(t+5\cdot\Delta t)$. Then, during the implementation of the convolution from Equations (8) to (11), $\chi(t)$, $\overset{\infty}{\chi}(t+\Delta t)$, …, $\overset{\infty}{\chi}(t+5\cdot\Delta t)$ can be regarded as a complete sequence, completed together through iterative loops.

As mentioned earlier, the goal of the newly proposed method is to make a prediction again based on the first prediction value (tomorrow). Thus, compared to the traditional method that starts from Equation (3), the newly proposed method begins the first step of convolution from Equation (8). In Equation (8), $\overset{\infty}{\chi}(t+\Delta t)$ and the subsequent prediction values are together, and $p(t)$ is the unique rapid observation value provided by USNO or IERS. However, $\chi(t)$ has 72 results, making the choice of $\overset{\infty}{\chi}(t+\Delta t)$ and $\chi(t)$ crucial for the accuracy of the convolution. It is known from Equations (4) and (5) that both have a half relation to $\overset{\in}{\chi}(t+\frac{\Delta t}{2})$. Part of $\overset{\in}{\chi}(t+\frac{\Delta t}{2})$ comes from the Day 1 prediction using IGU data in the PM domain, while another part comes from the separate Day 1 prediction of the EAM in the excitation domain. Clearly, the accuracy of the separate forecast is higher, which provides a better foundation for the selection of the initial value for convolution.

By keeping one value of $\chi(t)$ constant, or matching it with the 72 results of $\chi(t)$, and calculating all the convolutions from Equations (8) to (11), we can obtain 73*72 results. Among these, using the EOP 14C04 series at the prediction position as the reference true value, we calculate the MAE for each result. Finally, by summing each result and selecting the smallest MAE, we obtain our target optimal convolution result. This is the second important finding of this study.

It is important to note that we conducted numerous experiments and obtained relatively optimal combination selection results. Specifically, in the PM *X*-direction, the determined combination scheme has its convolution initial value provided by Scheme 6 of GAM's $\chi(t)$ in Table 1, while the prediction values of GAM's $\overset{\infty}{\chi}(t+\Delta t)$ and beyond are provided by Scheme 2 in Table 1. Additionally, the first forecast value of EAM in the excitation domain is provided by Scheme 5 in Table 2. In the PM *Y*-direction, the determined combination scheme has its convolution initial value provided by Scheme 6 of GAM's $\chi(t)$ in Table 1. The prediction values of GAM's $\overset{\infty}{\chi}(t+\Delta t)$ and beyond are provided by Scheme 9 in Table 1. Additionally, the first prediction value of EAM in the excitation domain is provided by Scheme 1 in Table 2. Since EAM data currently have two sources, GFZ and ETH, when using GFZ's EAM data and based on the LS+AR+EAM method, this combination selection method is referred to as B1. Conversely, when using ETH's EAM and based on the LS +AR+EAM method, the corresponding method is referred to as B2.

3.3.5. Return to the Excitation Domain after Combining in the Polar Motion Domain

The convolution and deconvolution of the Liouville physical equation exist in complex form (Wilson 1985), where *X* is the real part and *Y* is the imaginary part, indicating that a change in one will inevitably influence the other. At the end of the

previous section, we provided the optimal combination schemes for both the X and Y directions. Thus, this study made a reasonable hypothesis. First, in the PM domain, the best 1–5 day prediction results for the X and Y directions were combined into a complex form. Then, it transitioned to the excitation domain to conduct forecasts for days 6–11. Finally, it convoluted back to the PM domain. Since this recursive method involves optimal combinations, future results are bound to benefit. This is the third significant finding of this study. When based on the LS+AR+EAM method and using this recursive method, it is denoted as C1.

3.4. Evaluation of Prediction Accuracy

In this study, absolute error (AE), MAE, and improvement percentage (IP) were chosen as evaluation metrics for prediction accuracy (Kalarus et al. 2010; Kur et al. 2024). The corresponding formulas are organized as follows:

$$\mathrm{AE}_i = |(P_i - Q_i)|, \tag{13}$$

$$\mathrm{MAE}_i = \frac{1}{n} \cdot \sum_{i=1}^{n} (|(P_i - Q_i)|), \tag{14}$$

$$\mathrm{IP}_z^w = \frac{(\mathrm{MAE}_z^i - \mathrm{MAE}_w^i)}{\mathrm{MAE}_z^i} \times 100\%, \tag{15}$$

where n is the total number of experiments, i is the prediction horizons, P_i is the prediction on day i, and Q_i is the observed reference on day i. MAE_z^i and MAE_w^i represent the MAE of method Z and method W, respectively, on day i, in mas. IP is the percentage improvement in prediction accuracy of method W with respect to method Z on day i, in %.

4. Results and Analysis

First, the results comparing the proposed method with the top two competitors (ID116, ID136, and ID138), during the 2nd EOP PCC period (2021 September 1–2022 December 28), are presented (Kur et al. 2024). Then, the comparison results of the proposed method with the official prediction products from IERS or USNO in the extended 2nd EOP PCC (2016 January 6–2022 December 28) are shown. Finally, the results are analyzed and discussed.

4.1. Under 2nd EOPPCC Conditions (70 weeks)

First, the operational period of the 2nd EOP PCC was described. Then, the missing file locations submitted by participants ID116, ID136, ID138, and ID200 during this period were enumerated. Finally, the missing location information for the proposed method during the experiment was explained in detail. See Table 3.

It should be further noted that the study pays special attention to the fairness and impartiality of the comparisons in the presentation of results. First, the input data for the last month is supplemented with daily updates from USNO or IERS to reflect the real-time environment at that period. Then, the results output by the proposed method are completed before 20:00 UTC every Wednesday, strictly adhering to the requirements of the 2nd EOP PCC. Finally, when comparing with participants ID116, ID136, ID138, and ID200, the comparisons are conducted individually, retaining the common weekly positions for both sides. Specifically, when comparing B1 and ID136, the missing positions of the forecast for weeks 1–13, 30, 31, 50, 52, 56, and week 24 were removed, allowing both to use 51 weeks for a fair comparison. The comparisons among other methods are similar. These comparison results are shown in Tables 4 and 5.

Table 3
Explanation of the Experimental Week Positions in the 2nd EOP PCC Period

Methods	UTC	Location of Total Weeks	Location of Missing Weeks	Number of Weeks Residual
ID116	<20:00	1–70	31	69
ID136	<20:00	1–70	1–13, 30,31,50,52,56	52
ID138	<20:00	1–70	1–35, 50,52,55,58,68	30
ID200	<20:00	1–70	none	70
A1	<20:00	1–70	24	69
A2	<20:00	1–70	24	69
B1	<20:00	1–70	24	69
B2	<20:00	1–70	24	69
C1	<20:00	1–70	24	69

Note. The 2nd EOP PCC ran from 2021 September 1, at 00:00 UTC to 2022 December 28, at 20:00 UTC, spanning a total of 70 weeks. The missing information for ID116, ID136, ID138, and ID200 in the upper part comes from the data set publicly released by the organizers (Śliwińska-Bronowicz et al. 2023). The five methods in the lower part are proposed by this study. The 24th week is missing because the GFZ's OAM forecast data set was incomplete for that week, specifically missing on 2022 February 9, which is the 40th file update of OAM in 2022.

In Tables 4 and 5, A1, A2, B1, B2, and C1 are all based on the LS+AR+EAM method proposed by Dill et al. (2019). Among them, A1 is a replication of Dill et al. (2019) if the details of determining the order of the AR model are ignored. Compared to A1, A2 only changes the second step of convolution. B1 is the combination selection method proposed by this study, while B2 uses the EAM forecast data set from ETH compared to B1. C1 is a method based on the results of B1, which returns to the excitation domain prediction after combining in the PM domain.

As seen from Tables 4 and 5, the most basic A1 method outperforms the top two competitors ID 136 and ID 138 in the X direction for the first five days. In the Y-direction, its accuracy is lower than that of the top two competitors, which may be related to the fact that the competition teams use a fixed

Table 4
MAE and Corresponding IP of *X*-direction in 2nd EOP PCC

Weeks(<20:00)	Methods	0 day ↓	1 days ↓	2 days ↓	3 days ↓	4 days ↓	5 days ↓	6 days ↓	7 days ↓	8 days ↓	9 days ↓	10 days ↓
68 weeks	ID116	0.061	0.295	0.441	0.549	0.617	0.752	0.977	1.262	1.581	1.891	2.163
68 weeks	A1	0.119	0.28	0.413	0.497	0.584	0.707	/	/	/	/	/
68 weeks	A2	0.031	0.218	0.385	0.468	0.56	0.682	/	/	/	/	/
68 weeks	B1	0.031	0.162	0.332	0.417	0.526	0.64	0.762	0.943	1.262	1.659	2.044
68 weeks	B2	0.031	0.159	0.344	0.465	0.6	0.733	0.902	1.1	1.37	1.706	2.059
68 weeks	C1	0.031	0.181	0.33	0.419	0.528	0.644	0.785	0.978	1.288	1.606	1.948
51 weeks	ID136	0.03	0.289	0.462	0.568	0.608	0.723	0.827	1.053	1.322	1.639	1.984
51 weeks	A1	0.128	0.306	0.449	0.523	0.578	0.701	/	/	/	/	/
51 weeks	A2	0.03	0.229	0.409	0.487	0.541	0.666	/	/	/	/	/
51 weeks	B1	0.03	0.139	0.314	0.406	0.481	0.584	0.685	0.874	1.231	1.633	2.011
51 weeks	B2	0.03	0.133	0.325	0.463	0.567	0.684	0.853	1.1	1.388	1.689	2.033
51 weeks	C1	0.03	0.16	0.317	0.415	0.486	0.59	0.736	0.972	1.278	1.536	1.855
51 weeks	IP^{B1}_{ID136}	0.00%	51.90%	32.00%	28.50%	20.90%	19.20%	17.20%	17.00%	6.90%	0.40%	−1.40%
30 weeks	ID138	0.173	0.367	0.521	0.619	0.756	0.9	1.005	1.073	1.268	1.508	1.679
30 weeks	A1	0.125	0.304	0.405	0.438	0.489	0.611	/	/	/	/	/
30 weeks	A2	0.033	0.227	0.357	0.392	0.437	0.573	/	/	/	/	/
30 weeks	B1	0.033	0.125	0.285	0.323	0.395	0.534	0.669	0.868	1.183	1.501	1.784
30 weeks	B2	0.033	0.104	0.259	0.366	0.515	0.659	0.849	1.085	1.389	1.682	1.961
30 weeks	C1	0.033	0.146	0.282	0.332	0.391	0.534	0.68	0.878	1.171	1.438	1.696
30 weeks	IP^{B1}_{ID138}	80.90%	65.90%	45.30%	47.80%	47.80%	40.70%	33.40%	19.10%	6.70%	0.50%	−6.30%
69 weeks	ID200	0.031	0.252	0.58	0.984	1.347	1.729	2.026	2.245	2.442	2.698	2.992
69 weeks	A1	0.12	0.28	0.41	0.49	0.577	0.699	/	/	/	/	/
69 weeks	A2	0.031	0.216	0.38	0.463	0.553	0.672	/	/	/	/	/
69 weeks	B1	0.031	0.162	0.333	0.419	0.526	0.637	0.762	0.942	1.254	1.638	2.019
69 weeks	B2	0.031	0.161	0.35	0.472	0.601	0.731	0.905	1.103	1.359	1.687	2.052
69 weeks	C1	0.031	0.182	0.334	0.424	0.529	0.643	0.79	0.985	1.289	1.597	1.926
69 weeks	IP^{B1}_{ID200}	0.00%	35.70%	42.60%	57.40%	61.00%	63.20%	62.40%	58.00%	48.60%	39.30%	32.50%

Table 5
MAE and Corresponding IP of *Y*-direction in 2nd EOP PCC

Weeks(<20:00)	Methods	0 day ↓	1 days ↓	2 days ↓	3 days ↓	4 days ↓	5 days ↓	6 days ↓	7 days ↓	8 days ↓	9 days ↓	10 days ↓
68 weeks	ID116	0.071	0.182	0.256	0.358	0.426	0.522	0.621	0.771	0.973	1.163	1.329
68 weeks	A1	0.106	0.176	0.285	0.367	0.435	0.537	/	/	/	/	/
68 weeks	A2	0.047	0.136	0.24	0.329	0.408	0.511	/	/	/	/	/
68 weeks	B1	0.047	0.14	0.215	0.288	0.366	0.475	0.599	0.721	0.891	1.091	1.262
68 weeks	B2	0.047	0.133	0.243	0.344	0.41	0.484	0.585	0.691	0.835	0.995	1.154
68 weeks	C1	0.047	0.147	0.225	0.293	0.373	0.472	0.61	0.714	0.87	1.078	1.219
68 weeks	IP^{B1}_{ID116}	33.80%	23.10%	16.00%	19.60%	14.10%	9.00%	3.50%	6.50%	8.40%	6.20%	5.00%
51weeks	ID136	0.046	0.165	0.241	0.333	0.43	0.552	0.672	0.799	0.911	1.053	1.217
51weeks	A1	0.105	0.19	0.299	0.382	0.452	0.574	/	/	/	/	/
51weeks	A2	0.046	0.146	0.252	0.341	0.421	0.548	/	/	/	/	/
51weeks	B1	0.046	0.131	0.202	0.285	0.375	0.504	0.651	0.775	0.93	1.119	1.293
51weeks	B2	0.046	0.125	0.236	0.35	0.419	0.517	0.649	0.747	0.883	1.055	1.205
51weeks	C1	0.046	0.139	0.215	0.294	0.38	0.501	0.649	0.749	0.901	1.094	1.216
51weeks	IP^{B1}_{ID136}	0.00%	20.60%	16.20%	14.40%	12.80%	8.70%	3.10%	3.00%	−2.10%	−6.30%	−6.20%
30 weeks	ID138	0.103	0.308	0.395	0.459	0.569	0.716	0.873	1	1.153	1.371	1.557
30 weeks	A1	0.098	0.19	0.317	0.407	0.463	0.569	/	/	/	/	/
30 weeks	A2	0.042	0.151	0.272	0.361	0.422	0.543	/	/	/	/	/
30 weeks	B1	0.042	0.141	0.206	0.308	0.385	0.513	0.681	0.781	0.894	1.065	1.238
30 weeks	B2	0.042	0.129	0.249	0.389	0.413	0.486	0.66	0.791	0.925	1.083	1.259
30 weeks	C1	0.042	0.147	0.214	0.311	0.386	0.507	0.672	0.756	0.923	1.107	1.249
69 weeks	ID200	0.048	0.221	0.422	0.656	0.908	1.148	1.393	1.583	1.763	1.935	2.094
69 weeks	A1	0.106	0.177	0.289	0.368	0.431	0.531	/	/	/	/	/
69 weeks	A2	0.048	0.137	0.245	0.33	0.405	0.506	/	/	/	/	/
69 weeks	B1	0.048	0.139	0.217	0.287	0.363	0.469	0.595	0.719	0.889	1.089	1.263
69 weeks	B2	0.048	0.133	0.246	0.344	0.406	0.484	0.588	0.692	0.834	0.994	1.155
69 weeks	C1	0.048	0.145	0.226	0.291	0.37	0.467	0.608	0.714	0.87	1.077	1.22
69 weeks	IP^{B1}_{ID200}	0.00%	37.10%	48.60%	56.30%	60.00%	59.10%	57.30%	54.60%	49.60%	43.70%	39.70%

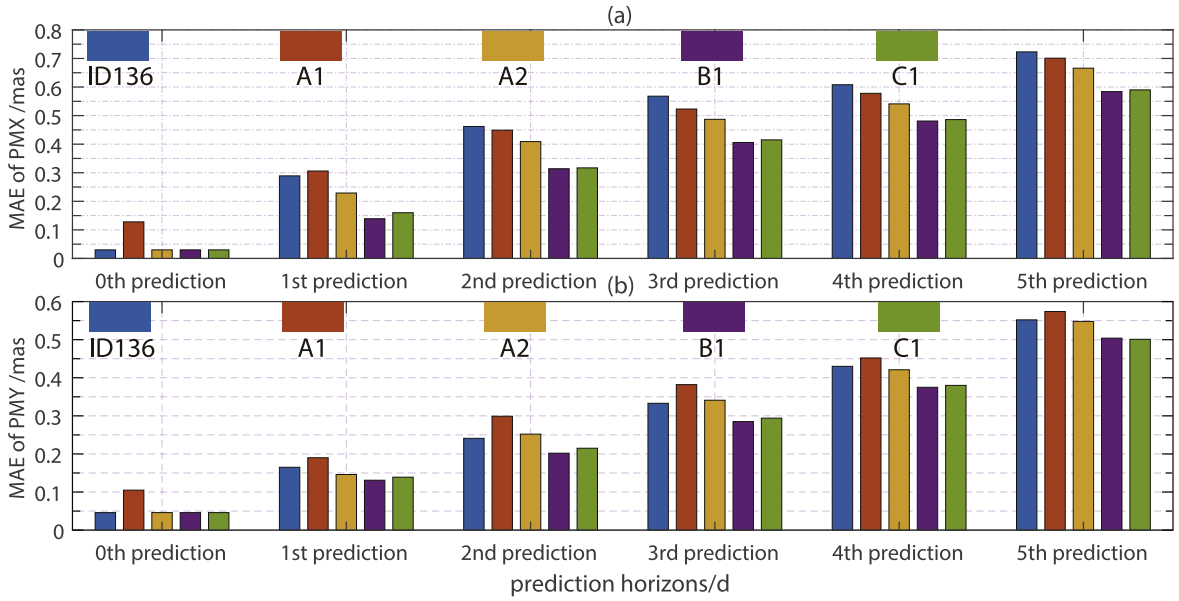

Figure 2. Bar figure comparison of the MAE for the first place (ID136), the traditional LS+AR+EAM method (A1), and the proposed methods (A2, B1, C1). (a) is the *X*-direction, (b) is the *Y*-direction.

order of the AR model. Then, comparing A1 and A2 shows that A2 consistently outperforms A1. On one hand, during convolution, the A2 method uses the rapid data updated by USNO or IERS on day 0 (today) instead of the PM value obtained through convolution for today. On the other hand, the starting point of A2's convolution is one step earlier than that of A1. In Figure 2, on day 0 (today), only A1 has the lowest accuracy, while ID136 and A2 have the same results on day 0, which again indicate that the A2 method is problem-free. For day 1 in Figure 2, the MAE of ID136 and A1 is not ideal, while the MAE of A2 is lower than that of both ID136 and A1. On one hand, it was mentioned earlier that day 1 of the A1 method is obtained by continuing the convolution based on the results of day 0, leading to its less than ideal results. On the other hand, the MAE of ID136 on day 1 is also not ideal, which we speculate may be due to the distant convolution starting point of ID136 and using the results of day 0 as the input for convolution. ID136 finally used rapid data updated by USNO or IERS separately to replace the results of day 0. However, as seen in Figure 2, compared to ID136, the B1 (in purple) has the lowest MAE from day 1 to day 5.

From Tables 4 and 5, it can be seen that ID138's day 0 values are 0.173 mas and 0.103 mas, rather than the 0.033 mas and 0.042 mas obtained from rapid data, which indicate that the starting point of ID138 during convolution is far from today, and this approach by ID138 inevitably leads to poorer results. However, on day 0, ID136 uses rapid data updated by USNO or IERS, consistent with the proposed method. Although ID116's accuracy on day 0 is insufficient, it may be because ID116 uses ESA's autonomous rapid data products. The results published by the 2nd EOP PCC show that ID136 ranks first and ID138 ranks second in the *X*-direction, while ID136 ranks first and ID116 ranks second in the *Y*-direction (Kur et al. 2024). Therefore, in Tables 4 and 5, the IPs of the proposed combination screening method (B1) relative to the top two in the competition were calculated. In Table 4, the IPs of the B1 method compared to the first place ID136 for days 1–7 are 51.9%, 32%, 28.5%, 20.9%, 19.2%, 17.2%, and 17%, respectively, indicating that the B1 method has a clear advantage. Similarly, in Table 5, the IPs of the B1 method compared to the first place ID136 for days 1–7 are 20.6%, 16.2%, 14.4%, 12.8%, 8.7%, 3.1%, and 3.0%, respectively, and the B1 method still has a certain advantage. These advantages are due to the closer convolution starting point of the B1 method. First, it predicts tomorrow's PM values (the first prediction) based on IGS ultra-rapid data (IGU) using various methods. Then, based on tomorrow's prediction, it generates a prediction for the future using various methods. Finally, convolution is used to obtain the final predicted results of PM. It is noteworthy that the convolution starting point of the B1 method is closer than that of A2, and Wei et al. (2024) have already verified that the first prediction accuracy based on IGU high-resolution is very high, thus providing good conditions for the initial convolution value of the B1 method. Additionally, the B1 method uses various cross-combination methods, which also provide constraints for a better initial convolution value. Therefore, the B1 method provides the best PM prediction results for days 1–7.

To more vividly compare the ID136 and B1 methods, Figure 3 illustrates the AE of their predictions. The left panels

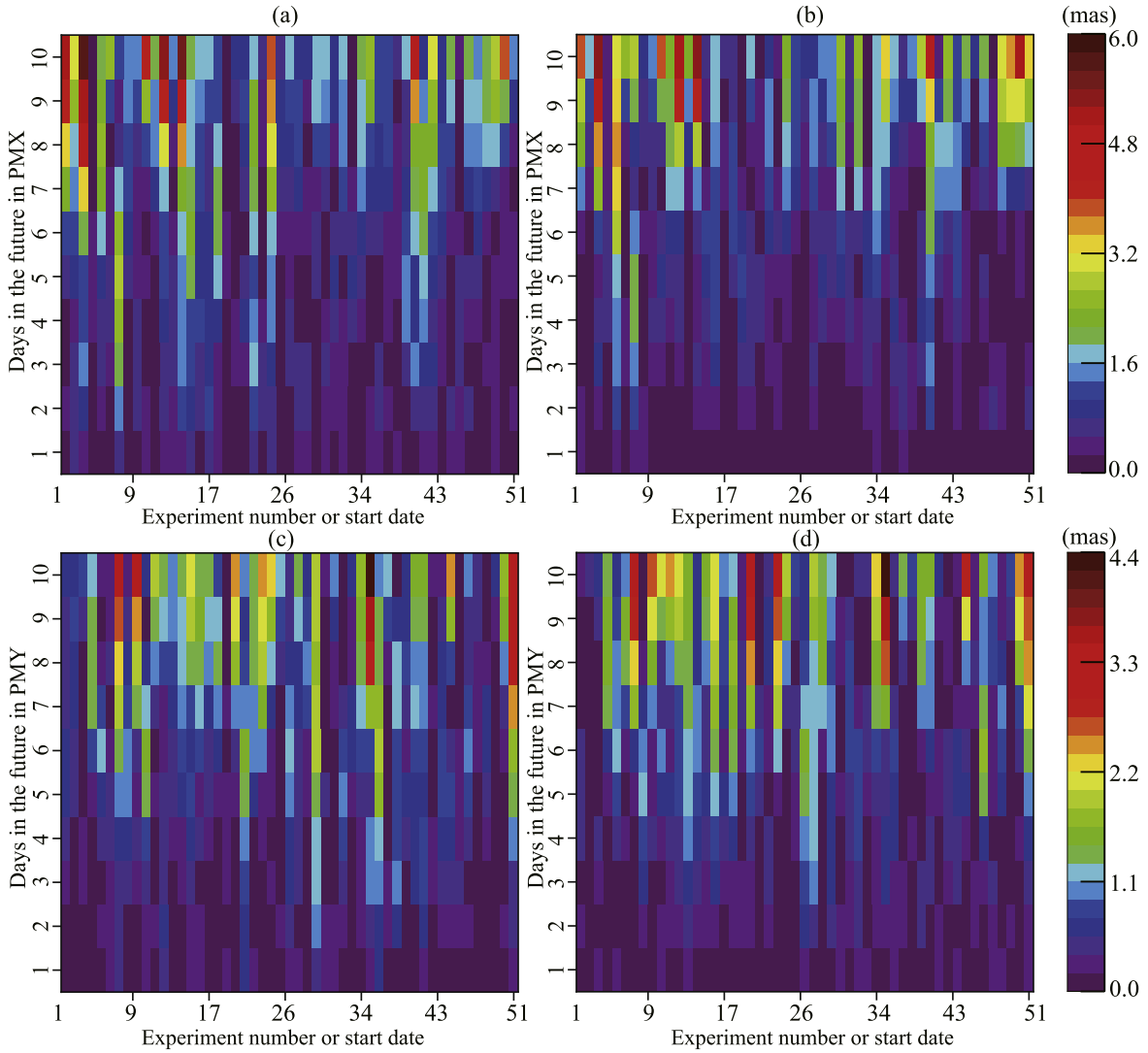

Figure 3. Comparison figure of the AE between the first place (ID136) on the left panels and the proposed methods (B1) on the right panels. (a) and (b) are the *X*-direction, (c) and (d) are the *Y*-direction.

show ID136, and the right panels show the B1 method, with the color reference standard on the far right. After comparison, it is evident that the prediction accuracy improvement of the B1 method is not only the best but also uniform. B1 has a stronger advantage in days 1–5 and a weaker advantage in days 6–10, with an overall distribution similar to ID136. Furthermore, Table 6 provides statistics on the maximum, minimum, and average AE for days 1–7. Compared to the first place (ID136), the proposed method (B1) is optimal in these three metrics.

The difference between the B2 and B1 methods is that the B2 method uses ETH's EAM forecast product, whereas the B1 method uses the commonly used EAM forecast product provided by GFZ. From Tables 4 and 5, it is evident that in the *X* direction, ETH's EAM forecast product offers no benefits and has a negative impact. In the Y-direction, due to the use of ETH's EAM forecast, positive improvements were observed in days 6–10. Additionally, there is the C1 method, which is based on the final results obtained from the B1 method. It combines them in the PM domain in a complex form and then returns to the excitation domain for prediction, obtaining results through convolution. In Tables 4 and 5, the C1 method appears ordinary, which may be related to the short interval of only 70 weeks that the 2nd EOP PCC ran. This shorter interval may not showcase the advantages of the C1 method. In the next section, the 2nd EOP PCC interval will be extended from 70 to 365 weeks, after which the C1 method will be analyzed.

ID200 is the official forecast product of USNO and is also relayed and updated by IERS. The last section of Tables 4 and 5

Table 6
AE Values of Statistical Methods ID136 and B1 Over 1–7 day Prediction Horizons

Time Span (days)	Methods	*X*-Minimum	*X*-Maximum	*X*-Mean	*Y*-Minimum	*Y*-Maximum	*Y*-Mean
1 day	ID136	0.003	0.72	0.289	0.004	0.582	0.165
1 day	B1	0	0.422	0.139	0.001	0.312	0.129
2 days	ID136	0.012	1.388	0.462	0.001	0.985	0.241
2 days	B1	0.006	1.182	0.314	0.005	0.585	0.207
3 days	ID136	0.005	1.928	0.568	0.017	1.196	0.333
3 days	B1	0.001	1.546	0.406	0.02	1.099	0.314
4 days	ID136	0.05	2.523	0.608	0.026	1.231	0.43
4 days	B1	0.062	1.956	0.481	0.001	1.272	0.403
5 days	ID136	0.027	2.717	0.723	0.059	1.699	0.552
5 days	B1	0.008	1.908	0.584	0.005	1.417	0.499
6 days	ID136	0.019	2.411	0.827	0.002	1.944	0.672
6 days	B1	0.001	2.735	0.685	0.02	1.575	0.598
7 days	ID136	0.003	0.72	0.289	0.004	0.582	0.165
7 days	B1	0	0.422	0.139	0.001	0.312	0.129

calculates the comparison of MAE between the proposed method and ID200, and the IP in prediction accuracy. From this, it can be seen that under the same output UTC time conditions, the proposed B1 method shows a clear advantage in 1–10 days.

4.2. Under Extended 2nd EOPPCC Conditions (365 weeks)

Under the conditions of the EOP PCC, the forecasting performance of the methods can be tested effectively. This is because the available data under these conditions are stringent, aligning with real-world environments, and can be directly applied to actual engineering projects. This is precisely the significance of conducting the 1st and 2nd EOP PCC. However, the 2nd EOP PCC only ran for 70 weeks, which was insufficient for testing the stability of the methods. Consequently, the extended 2nd EOP PCC forecasting accuracy evaluation period was from 2016 January 6 (the first Wednesday) to 2022 December 28 (the last Wednesday), totaling 365 weeks.

It should be noted that for the last month of the input data for the previous 295 weeks, the daily data updated by USNO or IERS were still used for concatenation, with the results output by 20:00 UTC every Wednesday. Since the daily data collected from 2016 January 6 onwards missed 15 weeks, the missing weeks are as follows: 47, 72, 75, 76, 85, 90, 92, 123, 124, 128, 155, 190, 213, 225, 232, and OAM in 2022 missed the 40th file (i.e., week 319). Therefore, the remaining number of experimental weeks is 349. The calculated MAE results are shown in Tables 7 and 8.

From Tables 7 and 8, it can be seen that due to the extended prediction accuracy evaluation period, the inclusion of more experiments makes the advantage of A2 over A1 more apparent. Similarly, the inclusion of more experiments also highlights the advantage of the C1 method, which performs best in the 6–10 day MAE, especially in the Y-direction. The B1 method shows the best overall MAE performance in the extended 2nd EOP PCC interval. Subsequently, the IP of B1 compared to the official prediction products (ID200) from USNO or IERS was calculated, with the IP of the B1 method being around 30% and exceeding 30% in the first 10 days. Furthermore, we converted Tables 7 and 8 into line graphs, as displayed in Figure 4. It can be clearly seen that the B1 method has a significant advantage over ID200. In terms of forecast accuracy over the 349 weeks interval, the B1 method achieves 0.735 mas and 0.505 mas on the 5th day, which is an excellent result in the field of PM prediction research.

To more thoroughly express the forecasting effectiveness of the B1 method across all prediction windows each year, Figure 5 illustrates the AE matrix for the B1 method and ID200. AE represents the absolute value of the difference between the predicted results and the final reference solution of the EOP 14C04 series, revealing event characteristics that schemes BC and Bulletin A cannot predict (Modiri et al. 2018; Dill et al. 2019). Meanwhile, the percentage for each color block interval was calculated. It is evident that Figure 5 includes Figure 3, with the results of Figure 3 appearing to the right of the black solid line in Figure 5. In Figure 5, the left panels show the results of ID200, and the right panels show the results of the B1 method. It is clearly visible that the B1 method has the smallest AE, and its distribution from 2016 to 2022 is relatively uniform. Focusing on the upper part (*X*-direction), the B1 method has a distribution percentage of 99.57% in the 0–5 mas range, with the AE for the first 5 days all below 2.5 mas. For the lower part (*Y*-direction), the B1 method has an AE below 1.25 mas in the first 3 days, with a distribution

Table 7
MAE and Corresponding IP of *X*-direction in Extended 2nd EOP PCC

Weeks(<20:00)	Methods	0 day ↓	1 day ↓	2 days ↓	3 days ↓	4 days ↓	5 days ↓	6 days ↓	7 days ↓	8 days ↓	9 days ↓	10 days ↓
349 weeks	ID200	0.049	0.255	0.558	0.904	1.224	1.534	1.837	2.084	2.343	2.614	2.875
349 weeks	A1	0.134	0.318	0.472	0.591	0.71	0.849	/	/	/	/	/
349 weeks	A2	0.049	0.243	0.415	0.546	0.672	0.805	/	/	/	/	/
349 weeks	B1	0.049	0.165	0.341	0.478	0.602	0.735	0.869	1.033	1.299	1.577	1.874
349 weeks	C1	0.049	0.186	0.348	0.474	0.598	0.724	0.86	1.032	1.295	1.566	1.862
349 weeks	IP^{B1}_{ID200}	0.00%	35.30%	38.90%	47.10%	50.80%	52.10%	52.70%	50.40%	44.60%	39.70%	34.80%

Table 8
MAE and Corresponding IP of *Y*-direction in Extended 2nd EOP PCC

Weeks(<20:00)	Methods	0 day ↓	1 day ↓	2 days ↓	3 days ↓	4 days ↓	5 days ↓	6 days ↓	7 days ↓	8 days ↓	9 days ↓	10 days ↓
349 weeks	ID200	0.045	0.194	0.395	0.63	0.881	1.11	1.309	1.468	1.599	1.736	1.877
349 weeks	A1	0.099	0.196	0.312	0.404	0.493	0.599	/	/	/	/	/
349 weeks	A2	0.045	0.156	0.272	0.364	0.458	0.569	/	/	/	/	/
349 weeks	B1	0.045	0.137	0.223	0.306	0.403	0.505	0.626	0.785	0.964	1.137	1.291
349 weeks	C1	0.045	0.151	0.233	0.306	0.408	0.506	0.628	0.762	0.924	1.103	1.238
349 weeks	IP^{B1}_{ID200}	0.00%	29.40%	43.50%	51.40%	54.30%	54.50%	52.20%	46.50%	39.70%	34.50%	31.20%

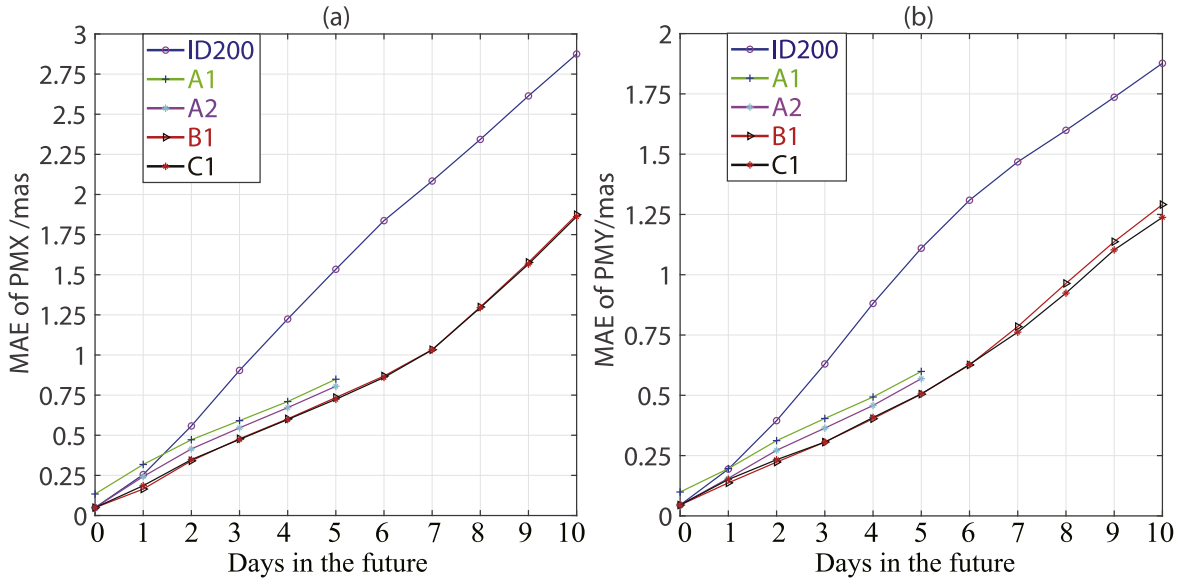

Figure 4. Comparison figure of MAE for the proposed methods (A2, B1, C1), the traditional LS+AR+EAM (A1) method, and ID200. (a) is the *X*-direction, (b) is the *Y*-direction.

percentage of 97.95% in the 0–2.5 mas range. The above analysis reaffirms that the B1 method, selected through combination screening in Section 4.1, is not only highly competitive but also performs stably over an extended prediction accuracy evaluation period.

4.3. Discussion

Due to the one-month delay in the EOP C04 series, all experiments used the daily data released by USNO or IERS to compensate for the delay, and results were output every Wednesday at 20:00 UTC. When using the IGS ultra-rapid (IGU) data, only the first value updated at 15:00 by IGS was utilized. To strictly comply with the competition organizers' requirement of submitting results before 20:00 UTC, the second value updated by IGS at 21:00 was not used. Wei et al. (2024) discussed the impact of using four consecutively updated IGS values on the accuracy of the first prediction, showing that the closer the time to the IGU update, the higher the accuracy of the first prediction. Therefore, if the competition rules were not followed and the second IGU value was used, the prediction accuracy for the first few days would improve. In Section 4.1, a fair and impartial comparison was conducted individually with the top two competitors in the 2nd EOP PCC interval. In Section 4.2, a fair and impartial comparison was conducted with the official prediction product ID200 from USNO or IERS in the extended 2nd EOP PCC interval. Therefore, the approach of this study regarding input data and experimental settings is beyond dispute.

This study did not make deliberate adjustments to the length of input data, the number of periodic terms for fitting, or the specific values. The lengths of input data are 14,600 and 1461, respectively, and the periodic terms in the PM domain used fixed values for the Chandler, annual, and semi-annual terms, with an additional 13.7 day tidal term used in the excitation domain (Dill et al. 2019). The order of the AR model was determined using the Akaike information criterion (AIC) (Konishi & Kitagawa 2008). All these parameters are fixed, indicating that the proposed method is fully reproducible.

Regarding the method itself, if the strategy for determining the order of the AR model is ignored, Method A1 is a replication of Dill et al. (2019). Method A2 builds on Method A1 and emphasizes that the input for the convolution should use the rapid value updated today to participate in iterative convolution operations. Compared to A2, the convolution starting point in Method B1 goes further by first generating numerous predicted combinations for the first prediction (tomorrow), providing a large number of initial convolution values for Method B1 to choose from. It should be noted that the strategy for combination selection involves calculating the sum of the smallest MAE. Although the B1 method determined by this strategy lacks theoretical support, extensive experimental validation has been conducted on it. Validation was carried out not only over the 70 week interval of the 2nd EOP PCC operation but also over the extended 365 week interval, consistently demonstrating that the B1 method is highly competitive. At the same time, this indicates that the accuracy of the initial convolution values and the proximity to the convolution starting point are crucial for enhancing the accuracy of PM predictions.

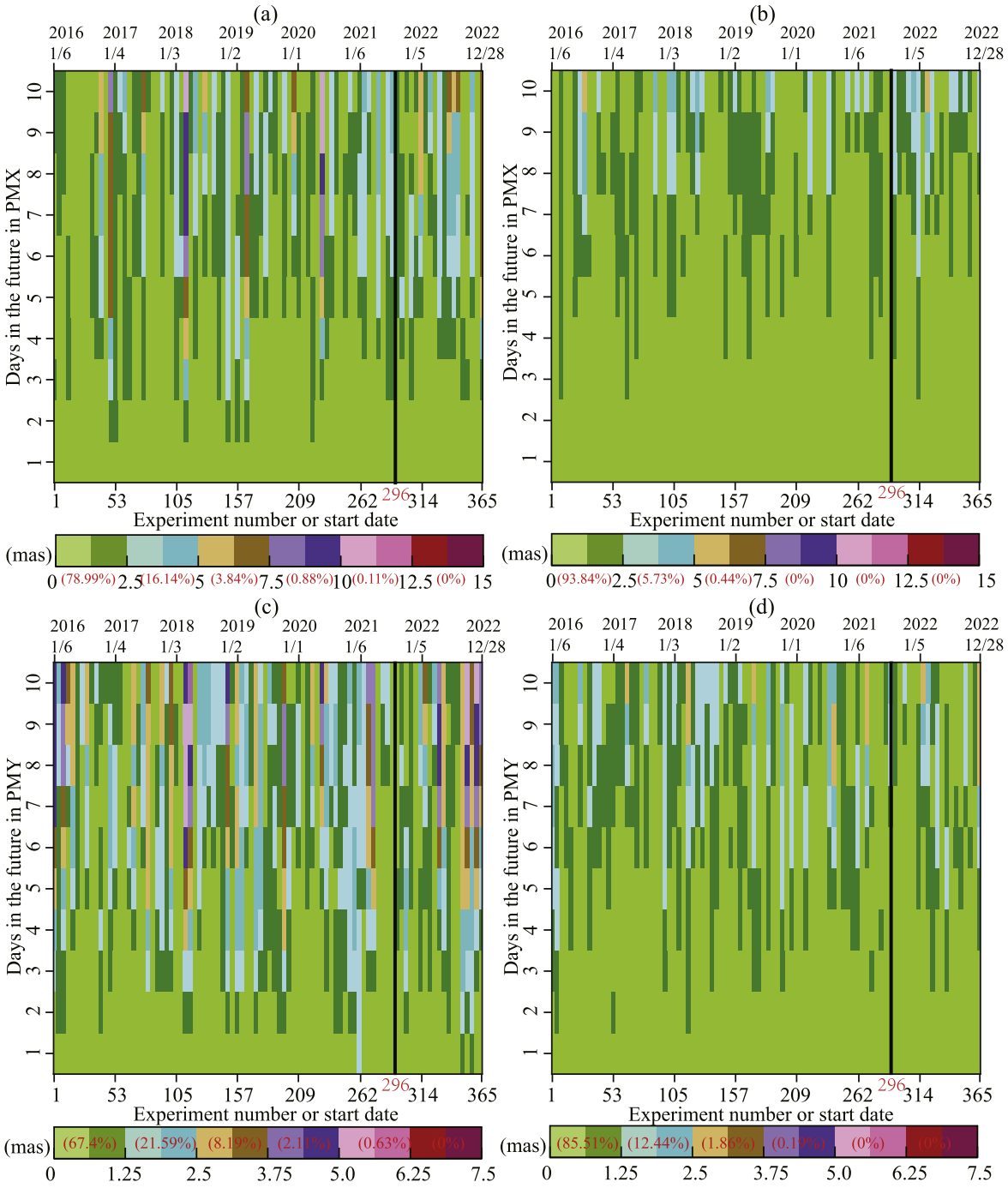

Figure 5. Comparison figure of the AE between the official prediction product ID200 from USNO on the left panels and the proposed method (B1) on the right panels. (a) and (b) are the *X*-direction, (c) and (d) are the *Y*-direction.

In the results analysis, only MAE and AE were used to quantify the accuracy of the prediction values relative to the reference values. However, the study lacks in quantifying the uncertainties inherent in the models and methods themselves, as well as in the propagation of errors to the prediction stage (Kiani Shahvandi & Soja 2022; Gou et al. 2024; Kiani Shahvandi et al. 2022, 2024a, 2024c, 2024b), and requires further research.

5. Conclusions

The LS+AR+EAM method by Dill et al. (2019) performed the best in the PM results of the 2nd EOP PCC (Kur et al. 2024). We conducted an in-depth analysis and study of the key convolutional steps in this method, and the conclusions are as follows:

The first result of the standard convolution (A1) is today's PM, which should be discarded in favor of using the high-precision rapid PM observations updated daily at 20:00 UTC by USNO or IERS. Meanwhile, the second result of the standard convolution (A1) should use the rapid PM observations as input, rather than using the first result of the standard convolution (A1) as input. The corrected method (A2) is superior to the standard convolution (A1), with more pronounced advantages in the first five days.

Considering the excellent accuracy of the first PM prediction based on high-resolution ultra-rapid data from IGS, multiple methods were used to obtain the first prediction in both the PM domain and the excitation domain. Meanwhile, compared to the A2 method, we advanced the starting point of the convolution by one step and, using the initial predictions (initial value of the convolution) obtained through various methods, aimed to minimize the sum of MAE to select the optimal convolution (B1). A fair and impartial comparison was conducted individually with the first place (ID136) in the 2nd EOP PCC interval, as well as with the official forecast product of USNO (ID200) in the extended 2nd EOP PCC interval. The B1 method showed significant advantages over 1–7 days, with these advantages diminishing as the prediction horizons increased. Additionally, we tested ETH's EAM forecast product, which only showed benefits after 6 days in the *Y*-direction. Furthermore, the results of the B1 method in the PM domain were combined in a complex form and returned to the excitation domain, showing a certain advantage after 6 days.

This study, through extensive experiments, verified that both the accuracy of the initial convolution values and the distance from the starting point of the convolution are crucial for improving the accuracy of PM predictions, and it has obtained a relatively optimal method for determining initial convolution values. In summary, the proposed method can effectively enhance user satisfaction with the 1–10 day PM prediction accuracy for applications such as deep space exploration and satellite autonomous navigation. In summary, the proposed method can effectively enhance user satisfaction with the 1–10 day PM prediction accuracy for applications such as deep space exploration and satellite autonomous navigation.

Acknowledgments

This work is supported by the Astrometric Reference Frame project (Grant No. JZZX-0102), the National Natural Science Foundation of China (NSFC, Grant Nos. 12473069, 12233010, and 12173070) and the Natural Science Foundation of Shanghai (Grant No. 24ZR1476800).

ORCID iDs

Wei Miao https://orcid.org/0000-0003-2584-1909

References

Altamimi, Z., Rebischung, P., Collilieux, X., Métivier, L., & Chanard, K. 2023, JGeod, 97, 47
Bizouard, C., Lambert, S., Gattano, C., Becker, O., & Richard, J.-Y. 2019, JGeod, 93, 621
Dill, R., Dobslaw, H., & Thomas, M. 2019, JGeod, 93, 287
Dill, R., Saynisch-Wagner, J., Irrgang, C., & Thomas, M. 2021, E&SS, 8, e02070
Dobslaw, H., & Dill, R. 2018, AdSpR, 61, 1047
Gou, J., Salberg, A.-B., Shahvandi, M. K., et al. 2024, arXiv:2412.17506
Gross, R. S. 2007, Treatise on Geophysics, 3, 239
Jia, S., Xu, T., & Yang, H. 2018, Acta Geodaetica et Cartographica Sinica, 47, 71
Jin, X., Liu, X., Guo, J., & Shen, Y. 2021, EP&S, 73, 1
Kalarus, M., Schuh, H., Kosek, W., et al. 2010, JGeod, 84, 587
Kehm, A., Hellmers, H., Bloßfeld, M., et al. 2023, JGeod, 97, 3
Kiani Shahvandi, M., Adhikari, S., Dumberry, M., et al. 2024a, NatGe, 17, 705
Kiani Shahvandi, M., Dill, R., Dobslaw, H., et al. 2023, JGRB, 128, e2023JB026720
Kiani Shahvandi, M., Mishra, S., & Soja, B. 2024b, EP&S, 76, 127
Kiani Shahvandi, M., Noir, J., Mishra, S., & Soja, B. 2024c, GeoRL, 51, 2024GL111148
Kiani Shahvandi, M., Schartner, M., Gou, J., & Soja, B. 2024d, Earth, Planets and Space (Berlin: Springer)
Kiani Shahvandi, M., Schartner, M., & Soja, B. 2022, JGRB, 127, e2022JB024775
Kiani Shahvandi, M., & Soja, B. 2022, AdSpR, 70, 563
Kong, Q., Han, J., Jin, X., et al. 2023a, G&G, 14, 368
Kong, Q., Han, J., Wu, Y., Wang, T., & Chen, Y. 2023b, GeoJI, 235, 1658
Konishi, S., & Kitagawa, G. 2008, Information Criteria and Statistical Modeling (New York: Springer)
Kosek, W. 2004, ArtSa, 39, 135
Kur, T., Śliwińska-Bronowicz, J., Wińska, M., et al. 2024, E&SS, 11, 2023EA003278
Malkin, Z., & Skurikhina, E. 1996, CIAAR, 93
Miao, W. 2023, Master's thesis, East China Univ. Technology
Mireault, Y., Kouba, J., & Ray, J. 1999, GPSS, 3, 59
Modiri, S., Belda, S., Heinkelmann, R., et al. 2018, EP&S, 70, 1
Noll, C. E. 2010, AdSpR, 45, 1421
Ray, J., Rebischung, P., & Griffiths, J. 2017, G&G, 8, 413
Schuh, H., & Behrend, D. 2012, JGeo, 61, 68
Schuh, H., Ulrich, M., Egger, D., Müller, J., & Schwegmann, W. 2002, JGeod, 76, 247
Shen, Y., Guo, J., Liu, X., et al. 2018, JGeod, 92, 333
Śliwińska-Bronowicz, J., Dobslaw, H., Kur, T., et al. 2023, GFZ Data Services,
Śliwińska-Bronowicz, J., Kur, T., Wińska, M., et al. 2022, ArtSa, 57, 257
Stamatakos, N., Luzum, B., Stetzler, W., & Schultz, E. 2009, in Proc. of the Journées 2008 "Systèmes de référence spatio-temporels" & X. Lohrmann-Kolloquium: Astrometry, Geodynamics and Astronomical Reference Systems
Su, X., Liu, L., Houtse, H., & Wang, G. 2014, JGeod, 88, 145
Sun, Z. 2020, PhD thesis, Shandong University
Wang, C., & Zhang, P. 2023, EP&S, 75, 153
Wang, G., Liu, L., Tu, Y., et al. 2018, StGG, 62, 243
Wang, Q. 2007, PhD thesis, Chinese Academy of Sciences
Wang, X.-Q., Du, L., Zhang, Z.-K., Liu, Z.-J., & Xiang, H. 2024, RAA, 24, 095019
Wei, N., Zhou, Y., Xu, X., et al. 2024, ChJG, 67, 1356
Wilson, C. R. 1985, GeoJI, 80, 551
Wu, K., Liu, X., Jin, X., et al. 2023, EP&S, 75, 179
Wu, Y., Zhao, X., & Yang, X. 2022, ArtSa, 57, 290
Xu, X., & Zhou, Y. 2015, AdSpR, 56, 2248
Xu, X., Zhou, Y., & Liao, X. 2012, JGeo, 62, 83
Zajdel, R., Sośnica, K., Bury, G., Dach, R., & Prange, L. 2020, GPSS, 24, 74
Zajdel, R., Sośnica, K., Bury, G., et al. 2021, JGeod, 95, 3